Biologically effective daily radiant exposure for erythema appearance, previtamin D₃ synthesis and clearing of psoriatic lesions derived from erythemal broadband meters at Belsk, Poland, for the period 1976-2023

Janusz W. Krzyścin[1], Agnieszka Czerwińska[1], Bonawentura Rajewska-Więch[1], Janusz Jarosławski[1], Piotr S. Sobolewski[1], Izabela Pawlak[1]

1 Institute of Geophysics, Polish Academy of Sciences, Warsaw, 01-452, Poland

Correspondence to: Janusz W. Krzyścin (jkrzys@igf.edu.pl)

Abstract. A long-term series of exposures to solar ultraviolet radiation (UVR) is required to assess the risks and benefits of radiation on different human biological processes. However, homogenisation of the amount of biologically effective solar energy (i.e. energy weighted according to the sensitivity of the selected biological process to solar radiation) reaching the Earth's surface over long periods is challenging due to changes in measurement methods and instruments. This paper presents the world's longest homogenised time series of biologically effective daily radiant exposures (DRE) from regular monitoring with different erythemal broadband radiometers (EBRs) operated at the Central Geophysical Laboratory of the Institute of Geophysics, Polish Academy of Sciences (IG PAS), Belsk (20.79°E, 51.84°N) from 1 January 1976 to 31 December 2023. The following biological effects were considered: erythema, cutaneous synthesis of previtamin D₃, and clearing of psoriatic lesions. The data for the latter two biological effects are estimated based on the proposed method of using EBR measurements to calculate other non-erythemal DRE. The following EBRs were used in the monitoring: Robertson-Berger meter (1975−1992), Solar Light model 501 (1993−1994 with #927, 1995−2013 with #2011) and Kipp &Zonen UV-AE-T #30616 from 5 August 2013 to the present. From 1976 to 2013, the homogenisation procedure consisted of comparing the measured erythemal DRE and daily maximum of UV index (UVI$_{MAX}$) with the corresponding modelled values from simulations using a radiation transfer model for cloudless conditions. Between 2014 and 2023, the EBR data were compared with data from a collocated reference instrument, the Brewer Mark II #64 spectrophotometer. Such comparisons resulted in a set of multipliers that were applied to the EBR measurements. Two different versions of the homogenisation method were applied analysing modelled and observed values for erythemal DRE and UVI$_{MAX}$ assuming different criteria for cloudless days. Three regression models of the erythemal data on common UVR proxy data (total column ozone, aerosol optical depth and global clear sky irradiance index) were used to reconstruct the UVR data from the beginning of the Belsk observations, allowing further validation of the homogenised UVR data. Linear trends calculated showed a statistically significant increase in erythemal annual and summer (June to August) radiant exposures of about 6 % per decade over the period 1976−2005. Thereafter, no trend was observed. Similar trend estimates were found for all biological effects considered.

The data are made freely available via the following repository: https://doi.org/10.1594/PANGAEA.972139 (Krzyścin et al., 2024). An additional version of the re-evaluated data, together with the corresponding clear sky and proxy data used in the UVR data reconstruction, is archived at:

37   https://doi.org/10.25171/InstGeoph_PAS_IGData_Biologically_Effective_Solar_Radiation_Belsk_1976_2023

38   (Krzyścin, 2024).

39   **Keyword(s**): erythemal broadband radiometer; biologically effective irradiance, homogenisation, radiant exposure

1 Introduction

40

41   Molina and Rowland (1974), winners of the 1995 Nobel Prize in Chemistry, argued that man-made

42   chlorofluorocarbons (CFCs), which were widely used in industry in the 1970s, could reach the stratospheric ozone

43   layer where they would be destroyed by short-wave ultraviolet radiation (UVR), releasing free chlorine atoms and

44   causing stratospheric O_3 depletion in a catalytic reaction cycle. Solar radiation in the shortest part of its spectrum

45   that reaches the Earth's surface (290−315 nm), known as UV-B, is strongly absorbed by stratospheric ozone. The

46   discovery of the ozone hole over Antarctica (Chubachi, 1984; Farman et al., 1985) and the predicted decreasing

47   trend in total column ozone (TCO_3) in other regions have stimulated interest in establishing continuous monitoring

48   of UV-B irradiance reaching the ground. In addition, there is growing evidence that such UVR trends can cause

49   various adverse health effects, such as skin cancers (including the deadly melanoma), DNA damage,

50   immunosuppression, oxidative stress and skin ageing (Neale et al., 2023).

51   Solar UV-B radiation from space is attenuated as it passes through the atmosphere due to light scattering (by cloud

52   particles, atmospheric gases and aerosols) and absorption (by O_3, NO_2, SO_2 and aerosols). The attenuation of light

53   increases with its path length through the atmosphere (i.e. usually described by the air mass), so solar elevation

54   and ground surface altitude are key parameters to consider in surface UVR modelling. Other factors forcing UVR

55   variability at the surface that are often used as proxies for atmospheric UV-B attenuation are total column O_3

56   (TCO_3) to account for UVR absorption by ozone, the clear sky index (CI) (i.e. a quotient of the all-sky global solar

57   irradiance (G) at the surface and the corresponding modelled clear-sky value (G_0) to account for combined

58   cloud/aerosol scattering effects on UVR), and aerosol optical depth (AOD) in the solar UV range (parameterising

59   UVR attenuation by aerosols). TCO_3 and G have been found to be the most important factors for modelling surface

60   UV-B radiation (Koepke et al., 2006, den Outer et al., 2010).

61   In the early 1970s, the broadband Robertson-Berger (RB) meter was developed to measure the biologically

62   effective (BE) UVR that causes skin redness, also known as erythema (Berger, 1976). The spectral characteristics

63   of RB resembled the erythemal sensitivity of human skin. RB instruments began continuous monitoring of

64   erythemal irradiance in 1974 at eight sites in the United States (Scotto et al., 1988). During the 1970s, instruments

65   were operated in other countries (Austria, Australia, Germany, Poland, Sweden, Switzerland) (WMO, 1977). At

66   the beginning of this global network, RB meters were calibrated using a travelling standard meter provided by the

67   Photobiology Center at Philadelphia University. After a few years, at some stations, including the Institute of

68   Geophysics, Polish Academy of Sciences (IG PAS) station at Belsk (51.84°N, 20.78°E), this calibration method

69   was replaced by comparisons with values modelled by a radiative transfer model. The Dave-Halpern model (Dave

70   and Halpern, 1976) was used to estimate erythemally weighted irradiance for cloudless sky conditions to calibrate

71   the Belsk data (Słomka and Słomka, 1985). Serious drawbacks of RB measurements were that their results were

72   reported in relative units (counts), temperature sensitivity, a lot of manual work in data preparation, sometimes

73   rapid ageing, and difficulties in accurately converting counts into the so-called sunburn unit (the minimum

74   erythemal radiation exposure that causes redness of the skin). These problems were significantly reduced in a new

75   version of the RB meter, a prototype of the current erythemal broadband radiometer (EBR), developed in the late

1980s as a result of collaboration between IG PAS and the Institute of Medical Physics of the University of Innsbruck (Blumthaler et al., 1989; Słomka and Słomka, 1993). Further prototype work at Solar Light (SL) Co. in Philadelphia resulted in the production of a commercial SL Biometer Model 501A, which replaced the RB meter. Other EBR versions were introduced in the 1990s, including those from Yankee Environmental Systems (Turner Falls, USA) and Kipp & Zonen (KZ) Co. (Delf, Netherlands). However, there was a need to standardise the correction procedure for the broadband UVR meters as it became apparent that the calibration provided by the manufacturer could not be relied upon even for the same type of instrument (Leszczynski et al., 1998). A standard calibration method that takes into account the individual spectral characteristics of the instrument and the loss of sensitivity has been proposed (Hülsen and Gröbner 2007). However, uncertainties of ~7 % can still be expected for well-maintained EBRs (Gröbner et al., 2009).

Long-term series of surface UVR from ground-based observations with a length of at least a few decades are rare. To the authors' knowledge, the longest UVR monitoring series began in Moscow in 1968 with a broadband (300−380 nm) instrument developed at the Moscow State University Meteorological Observatory (Chubarova et al., 2000). One of the world's longest measurements of solar UVR at the Earth's surface (and probably the longest taken by erythemal broadband instruments) are from Belsk. Measurements began in 1975 and continuous monitoring started on 1 January 1976. From a global perspective, the first UVR results appeared at the World Ozone and Radiation Data Centre (WOUDC) in 1989, but continuous UVR time series over three decades are only available for a limited number of stations including: Uccle (Belgium), Edmonton, Resolute, Toronto, Churchill, Saturna Island (Canada), Tateno (Japan) and Syowa (Antarctica) (WOUDC, 2025). The data archive of Network for the Detection of Atmospheric Composition Change (NDACC) also include stations with at least of three decades of UVR measurements such as Lauder (New Zealand), Mauna Loa (USA) and three Antarctica stations – Arrival Heights, Palmer Station and South-Pole (NDACC, 2025).

This article presents a retrospective evaluation of all UVR measurements (1976−2023) at Belsk made with different EBRs including: RB (1976−1992), SL Biometer model 501A (SL501A) (two instruments were used #927 and #2011 for the period 1993−1994 and 1995−2013, respectively) and KZ UV-AE-T #30616 (KZ616) from 5 August 2013 to the present. The re-evaluation for the period 1976−2013 is based on a comparison of the measurements with the modelled daily erythemal radiant exposure and the UV index at local solar noon from a radiative model simulation for clear sky conditions using TCO_3 and AOD measured at Belsk as model input parameters. The quality of the KZ616 data (2013−2023) will be accessed through comparisons with clear-sky erythemal irradiances simultaneously measured by the well-maintained Brewer spectrophotometer Mark II #64 (BS64). The details of the Brewer maintenance can be found in Czerwińska and Krzyścin (2024a). Erythemal daily radiant exposures (DRE) for the entire period of the UVR measurements at Belsk will be transferred to the corresponding vitamin D_3 and antipsoriatic DRE using a method proposed by Czerwińska and Krzyścin (2024a). A comparison of these DRE with those from BS64 spectral measurements in the period 2014-2023 will indicate the accuracy of the proposed reconstruction method of past BE data based on a statistical approach using typical proxies (TCO_3 and G) characterising atmospheric UVR attenuation. Finally, trend calculations for annual (January−December) and summer (June−August) radiant exposures (RE) for all biological effects considered and three versions of recalculated UVR data from 1976−2023 will be presented to confirm the robustness of the long-term changes in the BE radiation measured at Belsk.

2 Materials and Method

2.1 UVR monitoring

Recording of erythema irradiance with a standard RB meter (detector recorder No. 40) started in May 1975 at Belsk, but continuous monitoring began on 1 January 1976 and lasted until 1994. From May 1993, in parallel with the RB measurements, the monitoring of erythemal irradiance using the SL Biometer 501A #927 was initiated in order to establish monthly transfer coefficients for converting the RB output in sunburn units (SU) into erythemal units, i.e. the minimum erythemal dose (MED) causing skin redness in typical Caucasian skin, which was entered into the SL Biometer 501A measurements (Puchalski, 1995). MEDs were converted to the erythemal doses by multiplication with 210 J_{eryt} m^{-2}, where J_{eryt} denotes spectral irradiance integrated over time and wavelengths (290−400 nm) after weighting by the erythema action spectrum. Simultaneous measurements continued until December 1994, and all erythemal DRE measured with the RB meter before 1993 were multiplied by these transfer coefficients to produce data comparable to those obtained with the SL Biometer 501A.

As the RB meter showed sensitivity to ambient temperature, a correction for temperature effect was applied to the raw daily RB values (Borkowski, 1998) using empirical formulas proposed by Koskela et al. (1994). In addition, the RB Belsk series was also found to be affected by a change in calibration method in 1985, as the Dave-Halpern model (Dave and Halpern, 1976) calculations for cloudless conditions replaced field comparisons with the travelling standard instrument. This resulted in a downward step change of 14 % in the UVR series (Borkowski, 2000). The re-evaluated time series of erythemal DRE for the period 1976−1992 as made by Borkowski (2008) was archived and formed part of the Belsk's erythemal time series (1976−2023), which is further homogenised in this study.

Subsequent UVR measurements included SL501A # 927 (1993−1994) and #2011 (1995−2013), which were calibrated by the instrument manufacturer prior to shipment, but these calibrations proved to be very inaccurate Therefore, this paper is another attempt to recalculate past UVR data. In 2005, KZ616 was added to the IG PAS UV network and served as the reference instrument. It was not used for everyday UVR monitoring but only for occasional international calibration campaigns to provide a source for further calibrations with our SL biometers operating in Belsk and Hornsund (Spitzbergen). KZ616 started regular UVR monitoring on 5 August 2013, replacing the raw SL501A #2011, as BS64 (normally measuring TCO_3 and Umkehr ozone at Belsk since 1992) was established as the new UVR reference instrument for the IG PAS network, which has been in operation until now. The performance of KZ616 has proven to be very stable and it is still used in regular UVR monitoring.

In the following, we use the term "raw data" for the results of the EBR measurements in W m^{-2} and J m^{-2} that were previously archived in the internal databases of IG PAS before the release of the Krzyścin et al. (2024) and Krzyścin (2024) databases.

2.2 Ancillary data

Daily representatives of TCO_3 at Belsk are taken from the IG PAS data portal (Krzyścin, 2024), which contains results of daily average TCO_3 measurements, prepared for UVR modelling purposes. For example, the most reliable daily representative value of TCO_3 (marked with flag no. 1) was calculated as an average of the most accurate measurements (the so-called direct sun measurements) made by the Dobson spectrophotometer between 9:00 and 13:00 UTC. The least accurate case of ground-based TCO_3 observations (with flag no. 5) occurred under cloudy and low sun elevation conditions, i.e. before 9:00 and after 13:00 UTC. In this case, only the least reliable

154   Dobson observations were available for calculating the daily TCO_3 representative under overcast zenith and high

155   air masses. In the rare cases when ground observations were not available, satellite data (flag 6 or 7 depending on

156   the data source) and/or TCO_3 reanalysis data (flag 8) were used.

157   The daily representative of CI, DCI, which is further used in regression models (Sect. 2.3.4), is calculated as the

158   quotient of the daily integrals (sunrise to sunset) of G and G_0. Typically, the former values were obtained from

159   routine monitoring of global solar irradiance by various pyranometers (since 1965) including the following

160   instruments: Kipp & Zonen CM 6, Sonntag PRM-2, Kipp & Zonen CM 5, Kipp & Zonen CM 11, and

161   Kipp & Zonen CM 21. The data were calibrated using the Polish national standard, which had previously been

162   adjusted to the world standard during inter-comparison campaigns at the World Radiation Centre in Davos,

163   Switzerland. In addition, the Campbell-Stokes sunshine recorder provided the duration of sunshine per day to pre-

164   select sunny days. All these data are archived in the IG PAS Data Portal (Krzyścin, 2024).

165   To validate the corrected UV observations at Belsk, the long-term variability of BE radiation was also obtained

166   from the UVR reconstruction models (Section 2.3) using proxies (TCO_3 and DCI) from the ground-based

167   observations and reanalysis datasets. The European Centre for Medium-Range Weather Forecasts (ECMWF) v5

168   (ERA5) reanalysis provides, in addition to many other variables, intra-day TCO_3 values, G_0, and G for the period

169   1940−2024, which are freely available on the ERA5 (2025) website. Also included are data (from 1 January 1980

170   to the present) downloaded from the Modern-Era Retrospective Analysis for Research and Applications version 2

171   (MERRA-2) database (GMAO, 2025) using the Giovanni data search tool, which is freely available on the

172   Giovanni (2025) website.

173   **Table 1. The Belsk's instruments and their working periods.**

Data	Instrument/data	Operation period	Reference
Daily ERE and UV Index	Robertson-Berger Meter	1976−1994	
	SL Biometer 501 A # 927	1992−1994	Krzyścin et al. (2024)
	SL Biometer 501 A # 2011	1995−2013	Krzyścin (2024)
	Kipp-Zonen UV-AE-T # 30616	2013−present	
TCO_3	Dobson Spectrophotometer # 84	1963−present	Krzyścin (2024)
	Ozone Monitoring Instrument (OMI)	2004−present	ESRL (2025)
	Ozone Mapping and Profiling Suite (OMPS) Nadir-Mapper (NM) instrument	2012−present	ESRL (2025)
SunDur	Campbell–Stokes sunshine recorder	1966−1968, 1970−1973, 1975−present	Krzyścin (2024)
G	Kipp CM 6	1965−1980	
	Sonntag PRM-2	1981−1987	
	Kipp&Zonen CM 5	1988−1991	Krzyścin (2024)
	Kipp&Zonen CM 11	1992−2010	
	Kipp&Zonen CM 21	2010−present	
AOD_{340nm}	Sonntag pyrheliometers	1976−2013	Krzyścin (2024)
	CIMEL CE 318-T	2004−present	
G and G_0	ERA5 reanalysis	1940−present	ERA5 (2025)
G_0	MERRA-2 reanalysis	1980−present	GMAO (2025)

174   Atmospheric aerosols can be significant drivers of surface UVR, especially under clear sky conditions (Krzyścin

175   and Puchalski, 1998). The column properties of aerosols can be obtained from ground-based observations and used

176   in the modelling of radiative transfer in the atmosphere. Aerosol properties are described by various characteristics

177 (e.g. including AOD, single scattering albedo, asymmetry factor). In this article, we use Belsk's AOD at 340 nm

178 (IG PAS Data Portal, Krzyścin (2024)), which is estimated from the Linke turbidity factor measurements with

179 Sonntag pyrheliometers between 1976 and 2013 (Posyniak et al., 2016) and from the co-located solar photometer

180 CIMEL CE 318-T (2004−2023) operating within the Aerosol Robotic Network (AERONET) (AERONET, 2025).

181 Other aerosol properties are kept constant and equal to their typical values for the rural site. Taking into account

182 climatology of the Belsk's aerosol characteristics (AERONET, 2025) values of 0.95 and 0.69 are taken for single

183 scattering albedo and asymmetry factor, respectively. Table 1 summarises the sources of the data used in this

184 paper.

185 **2.3 UVR models**

186 **2.3.1 Clear-sky model**

187 Radiative transfer model simulations for clear sky conditions are used to quantify and correct biases in the output

188 of the Belsk UVR radiometers. To speed up the calculations, look-up tables were obtained using the Tropospheric

189 Ultraviolet and Visible (TUV) Radiative Transfer Model (TUV, 2025). The TUV model, which was introduced

190 by Madronich (1993), has since been widely used in UVR simulations.

191 Modelled clear-sky values of BE (erythema, previtamin D_3 synthesis, clearing of psoriasis lesions) RE in day D,

192 $RE_{EFF,CS}(D)$ in $J_{EFF}\,m^{-2}$, and irradiance at local solar noon, $Ir_{EFF,CS,MAX}$, in $W_{EFF}\,m^{-2}$, respectively, are calculated

193 using the following formulas:

194 $$Ir_{EFF,CS}(t) = \int_{290\,nm}^{400\,nm} Ir_{CS}(\lambda, t)\, AS_{EFF}(\lambda)\, d\lambda \qquad (1)$$

195 $$RE_{EFF,CS}(D) = \int_{Sunrise(D)}^{Sunset(D)} Ir_{EFF,CS}(t)\, dt \qquad (2)$$

196 where $Ir_{CS}(\lambda, t)$ is the spectral irradiance at time t and at wavelength λ, and $AS_{EFF}(\lambda)$ denotes the action spectrum

197 for specific biological effect EFF: EFF=ERYT for erythema (CIE 2019), EFF=VITD3 for photosynthesis of

198 previtamin D_3 in human skin (CIE 2006), and EFF=PSOR for psoriasis clearing (Krzyścin et al., 2012). Figure 1

199 presents the action spectra used.
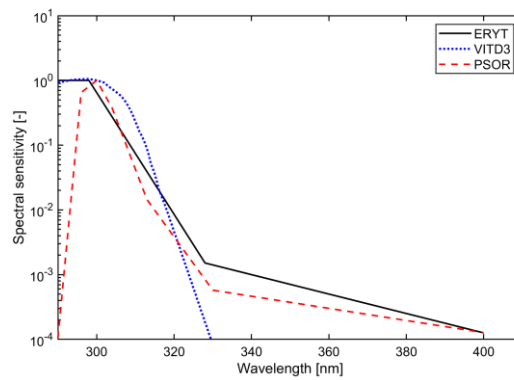
200 **Figure 1. Normalised action spectra for the specific biological effects: erythema (ERYT), photosynthesis of previtamin**
201 **D_3 in human skin (VITD3), psoriasis clearing (PSOR).**

202 Input to the clear-sky version of TUV model (daily representatives of TCO_3, annual and monthly mean AOD at

203 340 nm for the period 1976−2013 and 2014−2023, respectively) and output ($RE_{EFF,CS}(D)$ and $Ir_{EFF,CS,MAX}$ where

204 EFF={ERYT, VITD3, PSOR}), are archived in IG PAS Data Portal (Krzyścin, 2024).

2.3.2 Re-evaluation of the UVR measurements

Model simulations of erythemal DRE and UVI_{MAX} under cloudless sky provide a basis for the correction procedure of the past UVR data. A selection of clear-sky conditions throughout the entire day from the daily proxy values (relative sunshine duration and DCI), which were available for Belsk, is not straightforward as only the examination of the daily course of these measurements would allow to capture cloudless moments within the day. Thus, two different sets of correction coefficients are proposed, called CC1 and CC2.

The UVR measurements at Belsk from 1976 to 2023 can be clearly divided into three periods: 1 January 1976−31 December 1992, 1 January 1993−4 August 2013, and 5 August 2013−31 December 2023, according to the different broadband instruments used for UVR monitoring, i.e. RB, SL501A, and KZ616, respectively. For the first period, only the erythemal DRE were archived, whereas for other periods UVI_{MAX} was also available (equal to the value of erythemal irradiance at local solar noon during a cloudless day). There were also periods when both instruments were operated simultaneously for calibration purposes: March 1992−December 1994 (RB versus SL501A), 5 August 2013−31 December 2014 (SL501A #2011 versus KZ616), and 5 August 2013−31 December 2023 (KZ616 versus BS64).

The correction procedure before 5 August 2013 consisted of comparing the raw erythemal data with the corresponding modelled values obtained from the radiative model simulations (described in Sections 2.3.1) for days when ancillary data indicated that the sky was clear throughout the day. The LOcally Weighted Scatterplot Smoothing (LOWESS) proposed by Cleveland (1979) was used to extract the smoothed pattern of the multipliers of the raw UVR data, i.e. the correction coefficients (CCs), from the daily ratios between modelled and erythemal REs (for version CC1 of the correction) or from the ratios between UVI_{MAX} (version CC2). The following conditions were applied for the selection of clear sky data used in the two correction methods:

- CC1 – direct sun TCO_3 measurements occurred between 9:00−13:00 UTC (code 1 for the TCO_3 observation in IG PAS Data Portal, Krzyścin (2024)) and the daily difference between the observed and the theoretical maximum sunshine duration is less than 30 minutes at solar zenith angles (SZAs) less than 85°. This limit was chosen because broadband UVR measurements at larger SZAs are unreliable and the Campbell-Stokes instruments starts when direct sun irradiance exceeded 120 W m^{-2}.

- CC2 – for TCO_3, the same condition was set as for CC1, and the ratio between the observed and theoretical sunshine hours (for SZA < 85°) is not less than 85 %. CC2 values have only been calculated for the period since 1 January 1993. Prior to this date, a re-evaluation of the RB data with a model mimicking the KZ radiometer measurements by Krzyścin et al. (2011) showed that the correction was not necessary, i.e. CC2=1. This choice is also confirmed here by the constant long-term patterns of the ratio between modelled and observed DRE in the period 1976-1992 (see Sect. 3.2.1 for more details).

The smoothing procedure was applied to the long (1976-2013) and short (1993-2013) UVR time series for the CC1 and CC2 versions, respectively. A small jump (~0.01) in the smoothed UVI_{max} ratio was found in January 1993 (Sect. 3.2.1), which further corroborates the selection of CC2 = 1 prior to 1993.

The CC1 and CC2 versions of the re-evaluated Belsk UVR data are stored in the following free-access data archives: https://doi.org/10.1594/PANGAEA.972139 (Krzyścin et al., 2024) and https://doi.org/10.25171/InstGeoph_PAS_IGData_Biologically_Effective_Solar_Radiation_Belsk_1976_2023 (Krzyścin, 2024), respectively.

2.3.3 Reconstruction of BE radiation from the erythemal data

Broad-band instruments for measurement of the erythemal irradiance can also estimate non-erythemal irradiance by multiplying the erythemal irradiance by the so-called conversion factors (CF_{EFF}) derived from spectral UVR measurements and/or radiative transfer simulations (Schmalwieser et al., 2022; Czerwińska and Krzyścin, 2024a):

$$Ir_{EFF}(t) = CF_{EFF}(TCO_3, SZA) \times Ir_{ERYT}(t), \tag{3}$$

where SZA denotes the solar zenith angle at time t. Following this concept, the daily radiant exposure for previtamin D$_3$ synthesis and psoriasis clearance in year (Y), month (M), and day of month (D) $RE_{VITD3}(Y, M, D)$ and $RE_{PSOR}(Y, M, D)$, respectively, were estimated using the daily conversion factor, CF_{EFF}^*, applied to the erythemal DRE ($RE_{ERYT}(Y, M, D)$):

$$RE_{EFF}(Y, M, D) = CF_{EFF}^*(TCO_3, DY) \times RE_{ERYT}(Y, M, D), \quad EFF = \{VITD3, PSOR\}, \tag{4}$$

where CF_{EFF}^* depends on TCO_3 and DY (day of the year corresponding to the current day {Y, M, D}). CF_{EFF}^* and CF_{EFF} values were obtained from radiative transfer model simulations. The time series (1976−2023) of the conversion factors, $RE_{EFF}(Y, M, D)$, and the corresponding value of the biologically effective irradiance at local solar noon, $Ir_{EFF,MAX}$, have been archived in the IG PAS Data Portal (Krzyścin, 2024).

2.3.4 Regression models

The CCs described in section 2.3.2 were obtained for cloudless conditions and applied to all-sky conditions, where the contribution of the diffuse part of the radiation increases with cloud cover and dominates under overcast conditions. It cannot be ruled out that the instruments used to monitor UVR at Belsk have their own specific characteristics for recording diffuse radiation, and that CF_{EFF}^* and CF_{EFF} in Eqs. (3−4) also depend on the combined characteristics of clouds and instruments. To test whether this is the case, we investigated how different regression models, which were trained using the UVR data collected between 2014 and 2023 (for this period, the quality of the broadband radiometer was confirmed by the Brewer Mark II observations), reproduce the daily doses of erythemal radiation throughout the 1976-2023 monitoring period.

The first model (Mod1) is based on clear-sky spectra determined with the RT model discussed in Section 2.3.1 and a cloud modification factor (CMF) derived from DCI data. The second and third models (Mod2 and Mod3) are based on TCO$_3$ and DCI data evaluated on a monthly basis. TCO$_3$ and DCI were either taken from observations at Belsk (Mod2) or ERA5 reanalysis (Mod3).

According to a widely used UVR modelling concept (e.g. Rieder et al., 2008; den Outer et al., 2010; Čížková et al., 2018; Czerwińska and Krzyścin, 2024b) the erythemal DRE on a given day {Y, M, D}, $RE_{ERYT}(Y, M, D)$, is the product of *CMF* (empirical function of DCI parameterising UVR attenuation by clouds) for that day, and the modelled clear-sky value $RE_{ERYT,CS}$ (Section. 2.3.1):

$$RE_{ERYT}(Y, M, D) = CMF(DCI(Y, M, D)) \times RE_{ERYT,CS}(Y, M, D), \tag{5}$$

CMF is calculated here as a power function with the regression coefficients, α and β, depending on SZA at local solar noon, SZA_N, for the day {Y, M, D}:

$$CMF(DCI(Y, M, D)) = \alpha[DCI(Y, M, D)]^\beta, \tag{6}$$

279   where estimates for the regression coefficients, α and β, were obtained from the 2014−2023 data when the KZ616

280   measurements were well matched to the BS64 data (Sect. 3.1). In *DCI* ($DCI=DG\,DG_0^{-1}$) calculation, the daily

281   integral of global solar irradiance, *DG*, is from observations at Belsk or ERA5, and its clear-sky equivalent, DG_0,

282   from ERA5 (before 1980), and thereafter the mean of ERA5 and MERRA-2 values.

283   The standard least-squares subroutine (Matlab function – *fitlm(x,y)*) provided the estimates for three arbitrarily

284   selected local solar noon (SZA_N) ranges (Table 2). These regression coefficients were used for the reconstruction

285   of the RE_{ERYT} time series for the entire period of UVR measurements (1 January 1976 up to 31 December 2023).

286   This model will be referred to as Mod1 in this paper.

287   **Table 2. Estimates of the regression coefficients, α and β, describing the attenuation of erythemal DRE by the empirical**

288   **model, Mod 1, defined by Eqs. (5−6), for the three ranges of local solar noon.**

Regression Coefficients					
α	β	α	β	α	β
$SZA_N < 45°$		$SZA_N \geq 45°$ and $< 60°$		$SZA_N \geq 60°$	
0.954	0.844	0.918	0.750	0.960	0.697

289   The next two regression models were trained using the monthly averages of erythemal DRE, $RE_{ERYT}(Y,M)$, for

290   month M in year Y (from 2014 up to 2023) averaging all available daily $RE_{ERYT}(Y,M,D)$ values in M month for Y

291   year. The corresponding long-term (2014-2023) monthly means, $RE_{ERYT}^*(M)$, is from the averages of all data for

292   this calendar month. The idea of these models is to explain relative changes in the erythemal monthly RE, i.e.,

293   $\Delta RE(Y,M) = 100\% \, (RE_{ERYT}(Y,M) - RE_{ERYT}^*(M))/RE_{ERYT}^*(M)$ with the corresponding relative changes in variables

294   X that affect UVR, $\Delta X(Y,M) = 100\%(X(Y,M) - X^*(M))/X^*(M)$, where $X(Y,M)$ is the monthly mean of *DG* or

295   TCO_3 in year Y and month M and $X^*(M)$ is the long-term monthly means for month M:

296   $$\Delta RE_K(Y,M) = a_K(M)\,\Delta DG(Y,M) + b_K(M)\Delta TCO_3(Y,M) + c_K,\qquad(7)$$

297   where K=OBS (for Mod2) and ERA5 (Mod3) are for the regression using the explaining variables from the

298   measurements at Belsk and ERA5 reanalysis, respectively. Finally, the modelled $RE_{ERYT,K}$ value is equal to:

299   $$RE_{ERYT,K}(Y,M) = RE_{ERYT,K}^*(M)\left(1 + \frac{a_K(M)\,\Delta DG(Y,M) + b_K(M)\Delta TCO_3(Y,M) + c_K}{100}\right),\qquad(8)$$

300   **Table 3. Coefficients of the multilinear regressions derived for each calendar month based on the explaining variables**
301   **from the measurements at Belsk (Mod2) and ERA5 reanalysis (Mod3) data for the period 2014−2023.**

Month:	Mod2			Mod3		
	a_{OBS}	b_{OBS}	c_{OBS}	a_{ERA5}	b_{ERA5}	c_{ERA5}
January	0.84	−0.77	−5.69	1.34	−1.22	−8.38
February	0.81	−1.12	−0.12	0.95	−1.40	−0.05
March	0.59	−0.93	−0.65	0.84	−0.98	−0.77
April	0.90	−0.85	−1.94	1.26	−1.22	−3.77
May	0.86	−2.00	1.14	0.86	−1.97	0.64
June	1.08	−0.87	−0.05	1.14	−0.83	0.11
July	0.69	−0.84	0.00	0.40	−0.99	−0.00
August	0.82	−1.46	−1.99	0.63	−2.05	−1.40
September	0.86	−0.79	−0.00	0.94	−0.97	−0.00
October	0.80	−1.12	−0.49	0.86	−0.45	−0.52
November	0.58	−1.15	−1.02	0.66	−0.73	−0.97
December	0.73	−0.23	2.11	1.28	2.61	0.77

302   Models defined by Eq. (8) were used to compare fluctuations in UVR data in periods with RB and SL501A

303   measurements relative to the long-term monthly means in these periods, $RE^*_{ERYT, K}(M)$, that were approximated

304   using the long-term averages of the measured $RE_{ERYT}(Y, M, D)$ values for the period 1976−1992 and 1993−2013,

305   respectively. The regression coefficients, a_K, b_K, and c_K, which were calculated using the standard least-squares

306   linear fit to the most reliable (2014−2023) data (Table 3), were applied to construct monthly time series for the

307   entire measurement period (1976−2023).

308   **2.4 Statistical methods**

309   Several standard statistical characteristics, which are calculated from the relative differences, z_i, between the

310   observed, x_i, and the value of the regression model, y_i, values expressed in percentage of the observed value, are

311   used to determine the level of agreement between two time series. These are as follows: mean relative deviation

312   (MRD), mean absolute deviation (MAD), standard deviation (SD), root mean square deviation (RMSD), and

313   Pearson's correlation coefficient (R):

314      $z_i = 100\% \frac{y_i - x_i}{x_i}$, $\quad i = 1, ..., N.,$ (9)

315      $MRD = \frac{1}{N} \sum_{i=1}^{N} z_i$,   (10)

316      $MAD = \frac{1}{N} \sum_{i=1}^{N} |z_i|$,   (11)

317      $SD = \left(\frac{1}{N} \sum_{i=1}^{N} (z_i - MRD)^2 \right)^{\frac{1}{2}}$,   (12)

318      $RMSD = \left(\frac{1}{N} \sum_{i=1}^{N} z_i^2 \right)^{\frac{1}{2}}$,   (13)

319      $R = \frac{\sum_{i=1}^{N} (y_i - <y>)(x_i - <x>)}{\left(\sum_{i=1}^{N} (y_i - <y>)^2 \right)^{\frac{1}{2}} \left(\sum_{i=1}^{N} (x_i - <x>)^2 \right)^{\frac{1}{2}}}$, $\quad <x> = \frac{1}{N} \sum_{i=1}^{N} x_i$, $<y> = \frac{1}{N} \sum_{i=1}^{N} y_i$,   (14)

320   Standard least-squares linear regression is applied to find the long-term tendency in the data. According to

321   Weatherhead et al. (1998), the standard error of the linear trend estimate, SE_{LS}, by standard least-squares approach

322   should be multiplied by the factor $F = \sqrt{(1 + R_{k+1})/(1 - R_{k+1})}$ to obtain the standard error corrected for the

323   autocorrelation (with a time lag of 1) in the trend residuals, $SE_{LS, COR}$, if the trend residuals are positively correlated

324   with the autocorrelation coefficient equal to R_{k+1}. F is set to 1 if the autocorrelation coefficient in the residual time

325   series is negative.

326      $SE_{LS, COR} = F \times SE_{LS},$ (15)

327   Further in the text (Sect. 3.3), the slopes of the regression line will be calculated by Matlab function – *fitlm(x,y)*,

328   and the corrected standard error of the slope, $SE_{LS, COR}$ for cases with $R_{k+1} > 0$, will be enlarged by the factor

329   proposed by Weatherhead et al. (1998) (see Eq. (15)).

330

3 Results

3.1 The re-evaluation of the UVR measurements since 5 August 2013

On 5 August 2013, data of KZ616 replaced the raw data of SL501A #2011, which had been routinely used for UVR monitoring since 1995, as its performance had deteriorated (Fig. 2). Following this change, a new correction procedure for the Belsk's UVR meter was introduced for early detection of instrument failure. Each month its output (erythemal irradiance) was compared with the corresponding output of the collocated BS64. An example of such a monthly comparison (for June 2023) is shown in the scatter plot between the BS64 and KZ616 erythemal irradiances measured under clear-sky conditions (Fig. 3a). In addition, Fig. 3b shows the monthly mean ratios between BS64 and KZ616 erythemal irradiance obtained during cloud-free periods from 2014 to 2023.
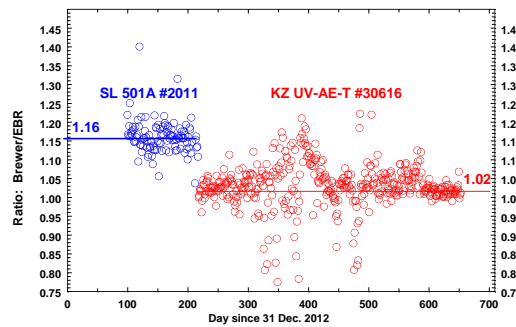
Figure 2. The ratio between the erythemal DRE from the erythemal radiometers (SL501A #2011 before 5 August 2013 and KZ616 afterwards) and the Brewer Mark II spectrophotometer for the 2013−2014 period. The horizontal lines denote the mean value of the ratio.
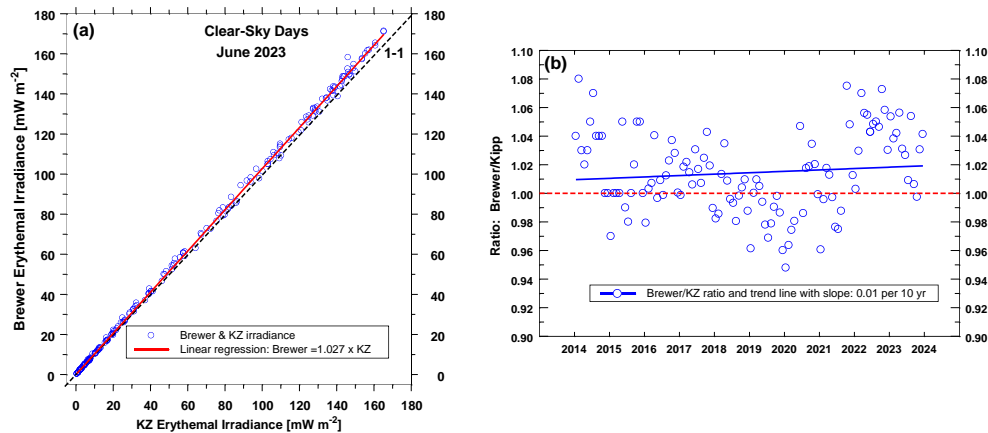
Figure 3. Comparison of the BS64 and KZ616 erythemal data for the period 2014−2023: (a) the erythemal irradiances measured by the BS64 versus corresponding output of KZ616 in June 2023 for clear-sky days, (b) time series of the monthly average of BS64/KZ616 ratios. The dashed line in Fig.3a shows the ideal 1:1 line.

Given the insignificant trend in the time series of the monthly BS64/KZ ratios (Fig. 3b), it was decided to keep the KZ616 data without additional adjustments. This assumption is also supported by the BS64/KZ616 comparisons as shown in the scatter plots of Fig. 4, which indicate that the Brewer and BE data cluster about the ideal 1:1 line. For the daily vitamin D_3 and antipsoriatic RE, the values were reconstructed from the daily erythemal RE using the transfer coefficients defined by Eq. (4) (the values are archived in the IG PAS Data Portal), but the

corresponding Brewer values were calculated from the real measured spectra weighted with the action spectra shown in Fig. 1.
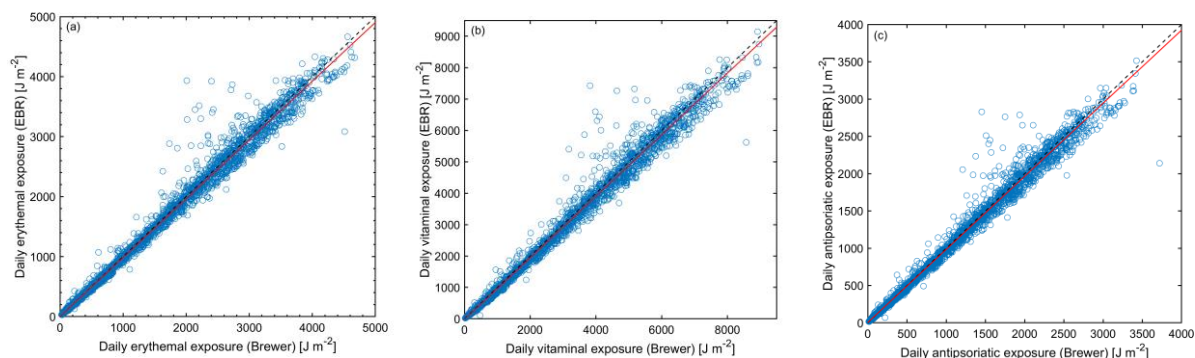
Figure 4. **Scatter plots (KZ616 versus BS64) for biologically effective DRE in the period 2014−2023: (a) erythema, (b) previtamin D₃ synthesis, and (c) psoriasis clearance.**

Additional support for keeping the KZ616 data without a correction provide Fig. 5 where the long-term (2014−2023) means of the monthly CC1 and erythemal DRE for each calendar month are shown in the upper and lower graphs of Fig. 5. The CC1 values are in the range of 1.00 to 1.02 during the period (April−September) when the intensity of solar UVR is usually high and the fine weather often allows prolonged outdoor activity
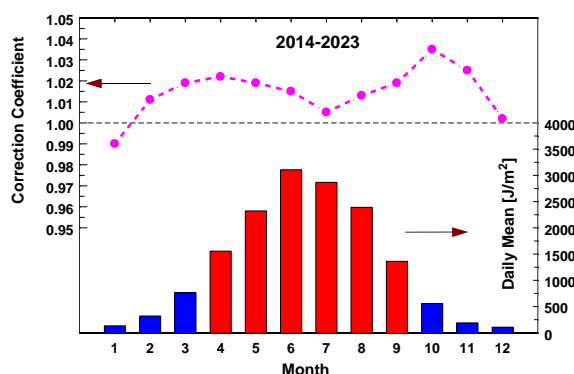
Figure 5. Seasonal pattern of the correction coefficient (CC1) and daily mean of erythemal RE for the period 2014−2023. Red bars denote months contributing mostly to the annual RE.

Table A1 shows the values of the descriptive statistics for the period 2014−2023 according to the different ranges of SZA values at local solar noon, which confirm the good agreement between the DRE for all considered biological effects from the well-calibrated BS64 and KZ616 measurements used in routine UVR monitoring. For example, regardless of the biological effect, MRD and RMSD are ~ −1 % and ~9 % for SZA_N <45°, which occurs from 8 April to 5 September at Belsk, i.e. during the period with the highest UVR intensity of the year. For SZA_N ≥ 60° (from 15 October up to 27 February of next year), MRD and RMSD are only slightly larger (~ −2 % and ~10 %, respectively) for the erythema and antipsoriatic exposures. These values are higher (~ −13 % and ~18 %) for the previtamin D₃ exposures, raising questions about the usefulness of the erythema radiometers for measuring vitamin D₃ exposure when SZA_N ≥ 60°. However, vitamin D₃ synthesis in the skin ceases during this period.

3.2 The re-evaluation of the UVR measurements before 5 August 2013

3.2.1 Correction coefficients from the clear-sky model simulations

Analyses of intraday UVR measurements in Belsk from 1 January 1976 to 4 August 2013 have to be divided into two parts, i.e. 1 January 1976−31 December 1992, and 1 January 1993−4 August 2013, due to the different broadband instruments used for UVR monitoring. In the first period, daily erythemal exposures were archived on the basis of manual summation of RB counts per day. For the latter period, 1-min erythemal irradiances were automatically recorded by a logger using SL501A biometers and utilized in the calculation of UVI_{MAX} and daily erythemal RE. Two methods of data correction were proposed (Sect. 2.3.2) using clear-sky data: modelled and measured daily erythemal RE (for the period 1976-2013) and UVI_{MAX} (1993-2013) for the correction method denoted CC1 and CC2, respectively. Figure 6 shows the time series of CC1 and CC2 values together with their smoothed values by the LOWESS smoother, which were used as multipliers of the raw UVR data before 5 August 2013.

UVI values were not archived between 1976 and 1992. This means that CC2 values cannot be calculated directly. However, CC2 values were assumed to be equal to 1 because the RB meter was previously adjusted to the SL501A #927 output using simultaneous measurements taken during the 1992–1994 period (Puchalski et al., 1995). Prior to 1992, CC2 =1 could be inferred from a flat CC1 pattern based on the daily erythemal RE. Using two sets of the re-evaluated 1976−2013 data will allow us to discuss the robustness of trend calculations for the entire 1976−2023 period of the UVR measurements at Belsk (Sect. 3.3).
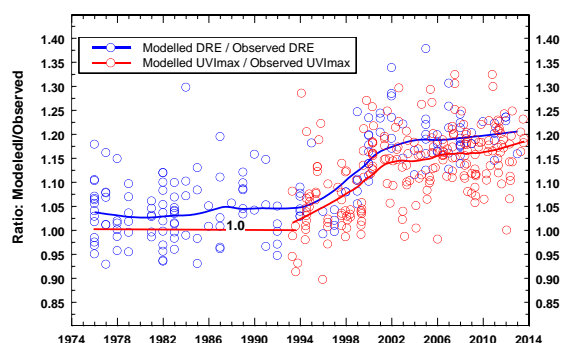
Figure 6. TUV model-observation ratios for erythemal DRE and UVI_{MAX} obtained for clear-sky days. The solid curves represent smoothed values of the ratios to be used as the correction coefficients, i.e., the multipliers applied to the raw measurements. The multipliers were set equal to 1 for the 1976−1992.

3.2.2 Performance of the regression models

Erythemal DRE for the period 1 January 1976 – 4 August 2013 were reconstructed with Mod1 defined by Eqs. (5−6). The model's constants came from the model training using the KZ data and the explaining variables (TCO_3 and DCI) from 5 August 2013 − 31 December 2023 period. The reconstructed values were compared with two sets of the re-evaluated data obtained before 5 August 2013 after multiplying raw daily erythemal RE with CC1 and CC2, respectively.
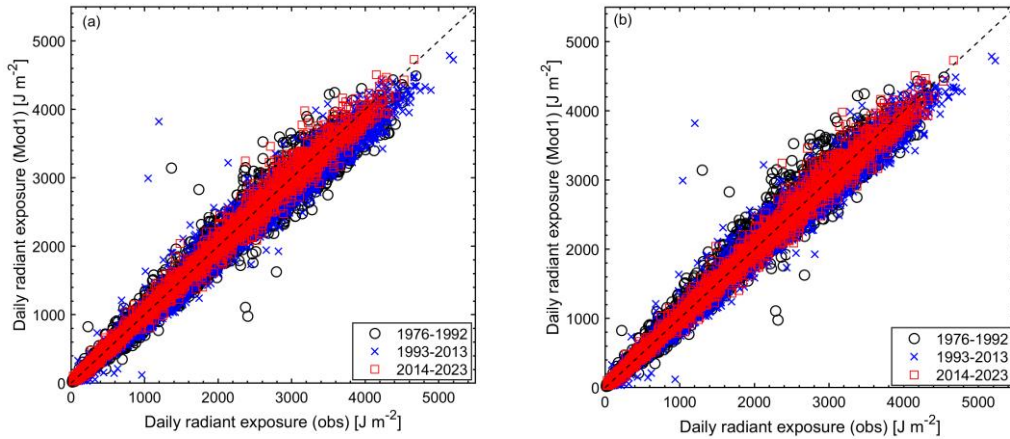
398 **Figure 7. Scatter plot of the modelled (Mod1) erythemal DRE versus the re-evaluated observed values for the**
399 **1976−1992, 1993−2013, and 2014−2023 period, respectively: (a) CC1 version of the correction coefficients, (b)**
400 **corresponding CC2 version of the correction coefficients. KZ616 measurements were taken without corrections.**

401 Figure 7 shows the scatter plot of the reconstructed (Mod1) versus re-evaluated erythemal DRE with CC1 (Fig. 7a)

402 and CC2 (Fig. 7b) multipliers of the raw data for the three periods corresponding to the RB, SL501A, and KZ616

403 measurements, respectively. The points in Figure 7 cluster around a line of perfect 1-1 agreement with only a few

404 outliers. It seems that there is only a small difference between the re-evaluated daily erythemal RE and the

405 corresponding output of Mod1 with the CC1 and CC2 multipliers. This is also supported by similar values of the

406 descriptive statistics for the periods 1976−1992 and 1993−2013 (Table 4). It is worth mentioning that the

407 performance of Mod1 in the period 2014−2023 is similar to that of the Brewer spectrophotometer that was found

408 when compared with the KZ616 data (note the close values of the descriptive statistics for the summer data in

409 column "CC=1" of Table 4 and Table A1 for the "$SZA_N<45^o$" cell and column "ERYT", for example, MAD values

410 are equal to 5.2 % and 5.3 %, respectively).

411 **Table 4. The descriptive statistics (MRD, MAD, RMSD, and SD) calculated from the relative daily differences,**
412 **100% (Mod1 value – re-evaluated measurement)/(re-evaluated measurement), for the periods 1976−1992, 1993−2013**
413 **and 2014−2023. The correlation coefficient R was obtained from the re-evaluated measurements and modelled values.**
414 **Two versions of the re-evaluated datasets were considered, using CC1 and CC2 multipliers on the raw measurements.**
415 **For the period 2014-2023, KZ616 data was used, which did not require adjustment. The results are shown for annual**
416 **(January−December) and summer (June−August) data.**

Statistics	Year-Round (January−…−December)					June−July−August				
	Multipliers of the raw data									
	1976−1992		1993−2013		2014−2023	1976−1992		1993−2013		2014−2023
	CC1	CC2	CC1	CC2	CC=1	CC1	CC2	CC1	CC2	CC=1
MRD	−2.7	1.6	−1.9	−0.3	1.4	−0.8	3.5	−2.6	−1.0	0.9
MAD	9.8	9.6	9.7	9.4	6.8	7.8	8.1	7.0	6.4	5.2
RMSD	13.7	14.1	14.5	14.6	10.5	10.8	11.7	10.1	9.7	6.9
R	1.00	0.99	1.00	0.99	1.00	0.96	0.96	0.97	0.98	0.98
SD	13.4	14.0	14.3	14.6	10.4	10.9	11.2	9.8	9.7	6.8

417

418 Erythemal DRE by Mod1 can be obtained for days when the explanatory variables, TCO_3 and DCI, are available

419 from the collocated measurements at Belsk by the Dobson radiometer and pyranometer, respectively. It is therefore

420 possible to fill gaps in the measured data and obtain a complete (1976−2023) series of erythemal DRE to be used

421 in calculations of erythemal annual and summer (June−July−August) RE. These REs can also be calculated using

the erythemal monthly RE based on Mod2 and Mod3. All these series are analysed in Sect. 3.3 for trend
calculations to assess the level of uncertainty in the long-term variability of the Belsk UVR data.

Table 5 shows the values of the descriptive statistics for the three models used (Mod1, Mod2 and Mod3) and two
versions of the re-evaluated data (using CC1 and CC2 multipliers on the raw data) based on the annual and summer
RE. The differences between descriptive statistics (MRD, MAD, RMSD, SD) in CC1 and CC2 columns are within
a few percentage points for MRD and about 1−1.5 percentage points for other statistics, indicating that the different
correction methods give fairly similar results. In most cases, Mod2 and Mod3 outperform Mod1 (see Table 5),
with smaller values of descriptive statistics. This is because these models are based on relative monthly differences
from the respective long-term means for the periods 1976−1992, 1993−2013 and 2014−2023. These means were
obtained by averaging the re-evaluated RB meter and SL501A, and the KZ616 data. The Mod1 model did not
apply a constraint on the average UVR in these sub-periods.

All models considered were designed to test whether changes in the primary UVR drivers, ozone and clouds,
explain year-to-year UVR variability. The performance of Mod3 is surprisingly similar to that obtained from Mod2
despite the use of UVR proxies (TCO$_3$ and DGI) from the ERA5 reanalysis.

The smallest correlation coefficients between the re-evaluated measurements and modelled values were found in
the period 1993−2013 for the measurement-model pairs with the same version of the CC multipliers (CC1 or CC2).
This is particularly pronounced for the summer data (see e.g. Mod3 values of 0.50 and 0.43 for CC1 and CC2
pairs, respectively), suggesting a poorer agreement between measurements and model in the period 1993−2013.
This was found for all models. However, other descriptive statistics (MRD, MAD, RMSD and SD) differed only
slightly, i.e. 1.5 percentage points, when values in CC1 and CC2 columns were compared.

Table 5. Same as Table 4, but the descriptive statistics are calculated using time series of erythemal annual and summer RE.

Statistics	Year-Round: January−…−December					Summer: June−July−August				
	Multipliers of the raw data									
	1976−1992		1993−2013		2014−2023	1976−1992		1993−2013		2014−2023
	CC1	CC2	CC1	CC2	CC=1	CC1	CC2	CC1	CC2	CC=1
					Mod1					
MRD	−3.3	0.9	−4.2	−2.6	−0.2	−1.9	2.4	−3.5	−1.9	0.5
MAD	3.9	2.5	4.7	3.2	1.0	4.0	3.4	4.4	2.8	1.8
RMSD	4.4	2.9	5.0	3.5	1.2	4.4	4.5	4.8	3.4	2.6
R	0.82	0.86	0.77	0.83	0.93	0.92	0.93	0.57	0.65	0.96
SD	3.2	3.0	2.8	2.4	1.4	4.2	4.0	3.3	2.9	2.7
					Mod2					
MRD	−0.9	−1.0	−0.5	−0.6	−0.3	−1.0	−1.1	−0.6	−0.6	0.0
MAD	2.1	2.0	2.0	1.8	0.6	3.3	2.9	2.2	1.9	1.3
RMSD	2.6	2.4	2.7	2.3	0.8	4.0	3.7	2.8	2.4	1.8
R	0.90	0.92	0.81	0.86	0.97	0.93	0.94	0.72	0.79	0.98
SD	2.6	2.4	2.7	2.3	0.8	4.1	3.7	2.8	2.4	1.9
					Mod3					
MRD	−0.4	−0.5	−0.9	−0.9	−0.6	0.2	0.1	−0.3	−0.3	0.1
MAD	1.5	1.4	2.7	2.8	0.8	3.0	3.2	2.9	2.9	2.1
RMSD	1.7	1.9	3.4	3.6	0.9	3.7	3.7	3.7	3.7	2.5
R	0.96	0.94	0.70	0.67	0.97	0.94	0.94	0.50	0.43	0.92
SD	1.8	2.0	3.4	3.5	0.8	3.9	3.9	3.8	3.8	2.7

3.3 Trend analyses

3.3.1 The erythemal annual and summer radiant exposures in the period 1976-2023

Trend analyses are applied to the erythemal annual and summer RE based on daily RE. There are two series to be considered when dealing with the measured data. The first, labelled OBS, uses only re-evaluated observations and the monthly average is calculated when at least 14 daily ERE values are available. The second one, OBS_F, contains all the daily gaps filled by Mod 1 simulations. For other models used there are no gaps. In the case of Mod1, the erythemal annual and summer RE are constructed using the results of the TUV model and the CMFs estimated from the DCI values. For Mod2 and Mod3, the monthly reconstructed RE values are summed over the year and summer season.

The 1976−2023 time series for the erythemal annual and summer RE using CC1 and CC2 correction multipliers are shown in Fig. 8 and Fig. A1, respectively. Fig.8a and Fig.8b are for the erythemal annual and summer RE with the use of CC1 but correspondingly Fig.A1a and Fig.A1b are based on CC2 values.

Linear regression lines are superimposed on the graphs to illustrate the long-term variability in the time series. Two independent lines are drawn to account for a change in the trend pattern observed in the time series somewhere in the early 2000s. The year of the trend change was calculated by examining the performance of fifteen combinations of this two-line pattern, varying the year of the trend change point (from 1995 to 2009). The best fit with maximum coefficients of determination was found for the trend change point in 2005. Therefore, the slopes of the regression lines (in kJ m^{-2} per year) and the trend values (in % per year) shown in Table 6 and Table 7, respectively, are calculated for the 1976−2004 and 2005−2023 periods. Standard errors of the trend estimates are calculated according to Eq. (15) accounting for the correction for the autocorrelation in the trend residuals if the autocorrelation coefficient with 1-yr lag, R_{k+1}, is positive (also shown in Tables 5−6).

The interannual variations and trend lines of erythemal annual RE are close to each other when comparing the upper graphs in Fig. 8 and Fig.A1. This can also be observed for the summers when comparing the corresponding lower plots. At the beginning of the RB observations (1976−1986), there were large oscillations from year to year, suggesting an instrumental problem with the data. As TCO$_3$ and cloud transparency data are available, it is important to analyse whether these large fluctuations are due to one or both of these two factors.

The slopes of the linear fit to the analysed time series (Table 6) show a statistically significant positive trend between 1976 and 2004 of around 20−30 kJ m^{-2} and 10−20 kJ m^{-2} per decade in the annual and summer data, respectively. The trends are mostly insignificant for the period 2005−2023, with only one exception (for the Mod1 data) with a continued positive trend of ~ 10 kJ m^{-2} per decade. The corresponding trend values expressed in dimensionless units (Table 7) have the same values of about 4−7% per 10 years in the former period for both the annual and summer time series. In the latter period, the positive summer trend from Mod1 is ~3 % per 10 years. Mod 1 and Mod 3 (with CC2) gave the lowest and highest trends, respectively. However, the differences between these trends are within the range of the uncertainty of the trend estimates at the 95% confidence level (as given by $T_c SE_{LS, COR}$ values in Table 6).
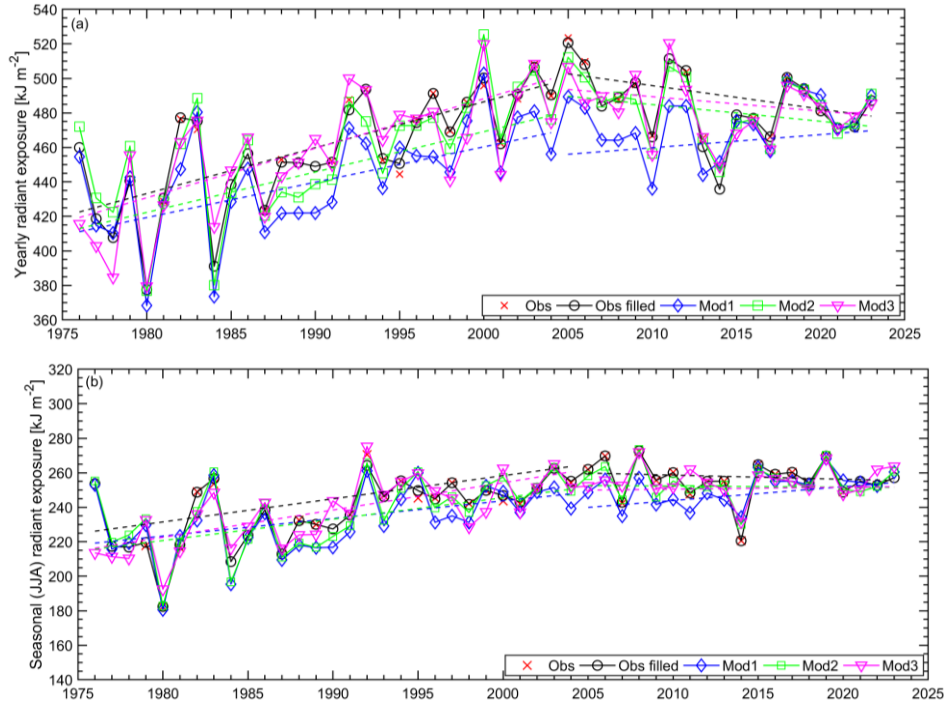
Figure 8. Time series (1976−2023) of the erythemal radiant exposures from re-evaluated observations (Obs), re-evaluated observations with filled gaps (Obs filled), and model estimates (Mod1, Mod2, and Mod3) using the CC1 version of the correction coefficients: (a) annual (January−December) radiant exposures; (b) summer (June−Aug) radiant exposures. Dashed lines represent the linear trends calculated for the period 1976−2004 and 2005−2023.

By averaging all available statistically significant annual and summer trend values shown in the third and seventh columns of Table 6 and Table 7, the following trends and their standard errors are obtained: for the period 1976−2004: 27.4 ± 4.4 kJ m^{-2} and 5.64 ± 0.92 % per decade for the erythemal annual RE, and 14.3 ± 4.3 kJ m^{-2} and 5.63 ± 1.03 % per decade for the erythemal summer RE. These values correspond to the average trend from the two series based only on the re-evaluated measurements (OBS$_F$ values in the Tables), i.e. 28.7 kJ m^{-2} and 5.9 % per decade for the erythemal annual RE, and 14.3 kJ m^{-2} and 5.6 % per decade for the erythemal summer RE.

Table 6. Trends (kJ m^{-2} per year) by the linear least-squares fit to the time series of erythemal annual and summer radiant exposures shown in Fig.8 and Fig.A1 calculated for the periods 1976−2004 and 2005−2023. SE$_{LS, COR}$ denotes the standard error of the trend estimate taking into account the autocorrelation R_{k+1} (with a lag of 1 year) in residuals of the trend model. Bold font indicates a statistically significant trend value at the 95% confidence level, based on the standard error of the trend multiplied by the corresponding critical T-value (T$_c$) for a two-sided probability. For the periods 1976–2004 and 2005–2023, T$_c$ is 2.05 and 2.10, respectively, with 28 and 18 degrees of freedom.

Data Type	Correct. Method	Annual (January...−...December) sum [kJ m^{-2}]				Summer (June−July−August) sum [kJ m^{-2}]			
		Trends$_{1976-2004}$		Trends$_{2005-2023}$		Trends$_{1976-2004}$		Trends$_{2005-2023}$	
		Trend ± T$_c$ SE$_{LS, COR}$	R_{k+1}	Trend ± T$_c$ SE$_{LS,COR}$	R_{k+1}	Trend ± T$_c$ SE$_{LS, COR}$	R_{k+1}	Trend ± T$_c$ SE$_{LS, COR}$	R_{k+1}
OBS$_F$	CC1	**2.66 ±1.07**	−0.11	−1.36 ±2.06	0.17	**1.34 ±0.76**	0.08	−0.24 ±1.03	−0.32
	CC2	**3.08 ±1.07**	−0.06	−0.45 ±1.83	0.14	**1.52 ±0.76**	0.07	−0.26 ±1.01	−0.30
Mod1	−	**2.05 ±1.17**	−0.19	0.76 ±1.64	0.08	**1.02 ±0.78**	−0.13	**0.80 ±0.76**	−0.20
Mod2	CC1	**2.34 ±1.25**	−0.16	−0.97 ±1.78	0.12	**1.24 ±0.80**	−0.08	−0.06 ±0.86	−0.38
	CC2	**2.84 ±1.25**	−0.10	−0.30 ±1.66	0.10	**1.50 ±0.80**	−0.01	0.29 ±0.86	−0.32
Mod3	CC1	**2.84 ±1.15**	−0.21	−0.84 ±1.60	−0.08	**1.58 ±0.66**	0.02	0.11 ±0.78	−0.13
	CC2	**3.34 ±1.11**	−0.22	−0.17 ±1.51	−0.13	**1.82 ±0.41**	0.05	0.46 ±0.76	−0.13

Table 7. Same as Table 6, but the results are for the trend values expressed in % per year.

Data Type	Correct. Method	Annual (January..−..December) sum [% yr⁻¹]				Summer (June−July−August) sum [% yr⁻¹]			
		Trends$_{1976-2004}$		Trends$_{2005-2023}$		Trends$_{1976-2004}$		Trends$_{2005-2023}$	
		Trend ± T_c SE$_{LS, COR}$	R_{k+1}	Trend ± T_c SE$_{LS, COR}$	R_{k+1}	Trend ± T_c SE$_{LS, COR}$	R_{k+1}	Trend ± T_c SE$_{LS, COR}$	R_{k+1}
OBS$_F$	CC1	**0.54 ±0.22**	−0.11	−0.28 ±0.36	0.17	**0.52 ±0.29**	0.08	−0.09 ±0.40	−0.32
	CC2	**0.64 ±0.22**	−0.06	−0.09 ±0.34	0.14	**0.60 ±0.29**	0.07	0.10 ±0.40	−0.30
Mod1	−	**0.42 ±0.25**	−0.19	0.16 ±0.31	0.08	**0.40 ±0.31**	−0.13	**0.31 ±0.29**	−0.20
Mod2	CC1	**0.48 ±0.27**	−0.16	−0.20 ±0.31	0.12	**0.49 ±0.31**	−0.08	−0.02 ±0.34	−0.38
	CC2	**0.59 ±0.25**	−0.10	−0.06 ±0.31	0.10	**0.59 ±0.31**	−0.01	0.11 ±0.34	−0.32
Mod3	CC1	**0.59 ±0.25**	−0.21	−0.17 ±0.34	−0.08	**0.62 ±0.25**	0.02	0.04 ±0.31	−0.13
	CC2	**0.69 ±0.22**	−0.22	−0.04 ±0.31	−0.13	**0.72 ±0.27**	0.05	0.18 ±0.29	−0.13

3.3.2 The vitamin D$_3$ and antipsoriatic annual and summer radiant exposures in the period 1976-2023

The commercial EBRs used to monitor erythemal irradiance can also measure non-erythemal irradiance (Czerwińska and Krzyścin, 2024a). Figure 4 and Table A1 provide that the daily vitamin D$_3$ and antpsoriatic RE derived from the KZ616 measurements agree with the directly measured BS64 values, as are the erythemal data obtained with KZ616. This supports the method of the transfer from erythemal irradiance to non-erythemal irradiance proposed by Czerwińska and Krzyścin (2024a).

Figure 9 shows the time series of annual and summer values of previtamin D$_3$ synthesis and psoriasis healing RE from 1976 to 2023. It appears that these time series are very similar. In addition, these time series are similar to the erythemal series shown in Fig.8. The correlation coefficients between the pairs of time series shown in Fig.8 and Fig.9, i.e. erythema & vitamin D$_3$, erythema & psoriasis, vitamin D$_3$ & psoriasis, were in the range [0.90, >0.999] with the lowest value for the erythema & vitamin D$_3$ and erythema & psoriasis pairs when the summer data from Mod1 simulations were considered.
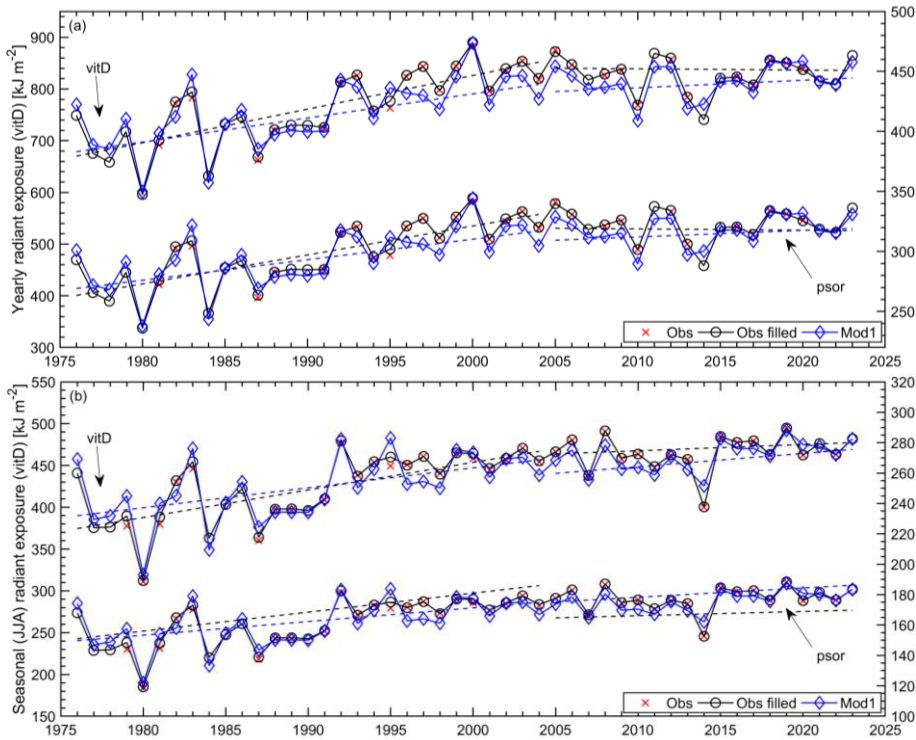
Figure 9. Time series (1976−2023) of the previtamin D₃ synthesis and psoriasis healing radiant exposures from re-evaluated observations (Obs), re-evaluated observations with filled gaps (Obs filled), and model Mod1 estimates (Mod1) using the CC2 version of the correction coefficients: (a) annual (January−December) radiant exposures; (b) summer (June-July-August) radiant exposures. Dashed lines represent the linear trends calculated for the period 1976−2004 and 2005−2023.

Table 8 shows the trend values for the period 1976-2004 and 2005-2023 from the time series calculated using the erythemal DRE multiplied by the transfer coefficients defined by Eq. (4). The transfer coefficients depend on only two parameters (TCO_3 and SZA), even on cloudy days, as previously shown by Czerwińska and Krzyścin (2024a). The statistically significant trend values for previtamin D₃ synthesis and psoriasis clearance are slightly higher, by about 1−1.5 percentage points per decade, than the corresponding trend values for the erythema shown in Table 7. Taking into account the uncertainty of the trend estimate of about 3% per decade, it cannot be said that the differences between the trends are statistically significant.

Table 8. Same as Table 7, but trend values are for previtamin D₃ synthesis and psoriasis clearance.

Data Type	Correct. Method	Annual (January−December) RE [% per year]				Summer (June−July−August) RE [% per year]			
		$Trends_{1976-2004}$		$Trends_{2005-2023}$		$Trends_{1976-2004}$		$Trends_{2005-2023}$	
		Trend ± T_c $SE_{LS, COR}$	R_{k+1}	Trend ± T_c $SE_{LS, COR}$	R_{k+1}	Trend ± T_c $SE_{LS, COR}$	R_{k+1}	Trend ± T_c $SE_{LS, COR}$	R_{k+1}
		Previtamin D₃ synthesis							
OBS_F	CC1	**0.70 ±0.25**	−0.12	−0.27 ±0.46	0.12	**0.64 ±0.33**	0.06	−0.07 ±0.42	−0.25
	CC2	**0.77 ±0.25**	−0.07	−0.03 ±0.40	0.08	**0.71 ±0.31**	0.05	0.16 ±0.40	−0.32
Mod1	−	**0.56 ±0.29**	−0.20	0.17 ±0.34	0.02	**0.51 ±0.33**	−0.15	**0.34 ±0.29**	−0.18
		Psoriasis clearance							
OBS_F	CC1	**0.66 ±0.25**	−0.13	−0.27 ±0.44	0.15	**0.63 ±0.31**	0.06	−0.07 ±0.42	−0.25
	CC2	**0.74 ±0.25**	−0.08	−0.03 ±0.42	0.10	**0.70 ±0.31**	0.05	0.16 ±0.40	−0.26
Mod1	−	**0.53 ±0.27**	−0.20	0.17 ±0.38	0.14	**0.51 ±0.33**	−0.15	**0.34 ±0.29**	−0.18

4 Summary and Discussion

Belsk is a unique observatory where UVR monitoring has been accompanied by monitoring of ozone (TCO_3), aerosol optical properties (AOD) and cloud characteristics (sunshine duration, DCI from global solar irradiance measurements), i.e. basic input parameters to a radiative transfer model allowing reconstruction of the erythemal RE. In addition, collocated BS64 measurements of UVR spectra are used in the frequent (every month) checking of actual KZ616 performance. BS64 spectral measurements also allow assessment of the quality of Czerwińska and Krzyścin (2024a) retrieval to convert standard erythemal measurements to the non-erythemal BE irradiance (see the cases of the vitamin D₃ and antipsoriatic DRE in Fig.4).

Two sets of raw UVR data multipliers (CC1 and CC2 as defined in section 2.3.2) have been proposed to correct and homogenise the time series of erythemal data. The re-evaluated time series appear quite similar, i.e. the difference between these series is within a few percentage points (Table 4 and Table 5). There was no need to re-evaluate the KS616 data for the period 2014−2023 because they agreed well with the BS64 data (Fig.3 and Fig.4). Regression models trained on the KZ616 data for the period 2014−2023 allowed the data to be reconstructed from the beginning of UVR observations at Belsk. These reconstructed series allowed independent examination of the pattern of interannual variability (which was unexpectedly large before 1985) and trends in the erythemal annual and summer RE. The regression models generally mimic the observed long-term variability in the re-evaluated

daily erythemal exposures. The statistically significant trend of ~6 % per decade with the standard error of ~1 % per decade for the period 1976−2005 is calculated (for both erythemal annual and summer RE) by averaging trends from the sample of seven versions of trend estimates from re-evaluated and reconstructed data (Table 7). All individual trend values in Table 7 are within the range 6% ± 2% (i.e. there is no outlier in this trend sample).

The uncertainty (at the 95% confidence level) of the individual trend estimates for the period 1976-2005 (Table 7) are of about 2-3% per decade, i.e. quite close to double the standard error of the mean trend derived from the sample. This supports the robustness of the trend estimates in annual and summer RE for the 1976−2005 parts of the Belsk time series. In addition, it also appears that the correction methods applied to the 1976−2013 raw UVR data, based on the comparisons of clear-sky erythemal DRE (CC1 method) and noon UVI (CC2 method), lead to differences in the individual 1976−2005 trend estimates of only about 1 % per decade (see Table 7 for the trend differences between pairs of OBS_F, Mod2 and Mod3 calculated with the CC1 and CC2 correction applied to the raw time series).

We found that our DRE estimates for all biological effects considered (erythema, vitamin D_3 and psoriasis) were close to those obtained from the Brewer's spectra with a bias of ~ −1 % and a standard deviation of ~ 9 % (Table A1) for the part of the year when UVR is of particular interest, when SZA at local solar noon is less than 45° (i.e. below the shadow length), according to the so-called shadow rule for protection against high UVR (Downham, 1998).

Krzyścin et al. (2011) found a trend of 5.6 % ± 0.9 % (1σ) per decade in the erythemal annual RE for the period 1976−2008. This is in good agreement with the present trend estimate, regardless of the very different correction methods used. The correction of the SL501A data carried out in 2011 was based on simultaneous measurements with KZ616 for the period 2008−2009 and further corrections for the instrument ageing using TUV cloudless sky simulations.

Similar trend estimates for erythemal radiation can be inferred from the reconstructed erythemal time series for the Moscow region based on the UVR measurements by the broadband (300−380 nm) radiometer (Chubarova et al., 2018) and the statistically reconstructed erythemal radiation series for Hradec Kralowe (Čížková et al., 2018). For the Moscow region, the authors reported a statistically significant positive trend of more than 5 % per decade for the period 1979-2015. Volpert and Chubarowa (2021) revealed the decadal trend in the reconstructed erythemal UV irradiance over the Moscow region for the warm season (May−September) of 5.1 % ± 1.1 % per decade in the period 1979−2016. Estimates from the smoothed pattern of annual erythemal exposures taken from Fig. 2c by Čížková et al. (2018) for 1976 (~1.20 kJ m^{-2} for the annual mean of erythemal daily RE) and 2005 (~1.40 kJ m^{-2}) give a trend of ~5% per decade for the period 1976−2004. From around 2005, both time series show a levelling off. Trends calculated here from the RE time series for other biological effects (previtamin D_3 synthesis and psoriasis lesion clearance), using an approach analogous to that used for the erythema data, show very similar trends.

5 Code and data availability

All data have been published as free access TXT files and are made available through PANGEA repository at https://doi.org/10.1594/PANGAEA.972139 (Krzyścin et al., 2024) and IG PAS Data Portal repository: https://doi.org/10.25171/InstGeoph_PAS_IGData_Biologically_Effective_Solar_Radiation_Belsk_1976_2023 (Krzyścin, 2024). ERA5 data are publicly accessible at https://cds.climate.copernicus.eu/datasets/reanalysis-era5-

single-levels?tab=overview (ERA5, 2025). MERRA-2 data are accessible at https://doi.org/10.5067/Q9QMY5PBNV1T (GMAO, 2025). Coefficients of the linear regression are calculated by Matlab function (Matlab R2018a) – *fitlm(x,y)*.

6 Conclusions

It is generally accepted that the use of a sample of time series containing different possible realisations of a time series increases the reliability of the results compared to the analysis of a single time series. Therefore, this study includes 7 time series (refer to number of analysed time series shown in Table 7) to discuss the reliability of year-to-year variability and trends in annual and summer biologically effective radiant exposures. This is beneficial for evaluating the quality of the data and establishing confidence in the results. Data archived in PANGEA (Krzyścin et al., 2024) and in the IG PAN Data Portal (Krzyścin, 2024), together with the results of three regression models, form the reliable basis for analysing UVR time series at Belsk for the period 1976–2023. The long-term variability of erythemal radiation calculated for Belsk corresponds to that previously recorded at distant stations in central/eastern Europe, making results of these future analyses applicable to wider areas. For example, the daily characteristics of BE radiation at Belsk seem to allow the development of scenarios for outdoor human activities, enabling people to obtain the maximum health benefits from sunbathing while minimising the risk of erythemal overexposure.

Appendix A

Table A1 presents descriptive statistics (defined in Sect. 2.4) of the relative differences between biologically effective DRE measured by the KZ616 and the BS64, $100\%(RE_{EFF, KZ616} - RE_{EFF, BS64})/RE_{EFF,BR64}$. The vitamin D_3 and antipsoriatic RE were reconstructed from the erythemal RE (Sect. 2.3.3), but the Brewer RE values were calculated using the daily integral of the measured spectral irradiance weighted by the action spectra (Fig.1).

Table A1. Descriptive statistics of the 2014-2023 relative differences between the daily biologically effective radiant exposure with the Kipp & Zonen erythema radiometer (UV-S-AE-T #30616) and the Brewer spectrophotometer #064 in percent of the Brewer data for the different SZA ranges at local solar noon.

Statistics	$SZA_N<45^o$			SZA_N [45°, 60°]			$SZA_N \geq 60^o$		
	ERYT	VITD3	PSOR	ERYT	VITD3	PSOR	ERYT	VITD3	PSOR
MRD	−0.6	−1.5	−0.7	−2.5	−6.6	−3.3	−1.7	−13.2	−1.7
MAD	5.3	6.0	5.6	4.9	7.9	5.4	6.8	14.7	7.0
RMSD	8.7	9.2	9.0	7.2	10.0	7.8	10.0	16.3	10.3
SD	8.7	9.1	9.0	6.8	7.6	7.1	9.9	9.5	10.2
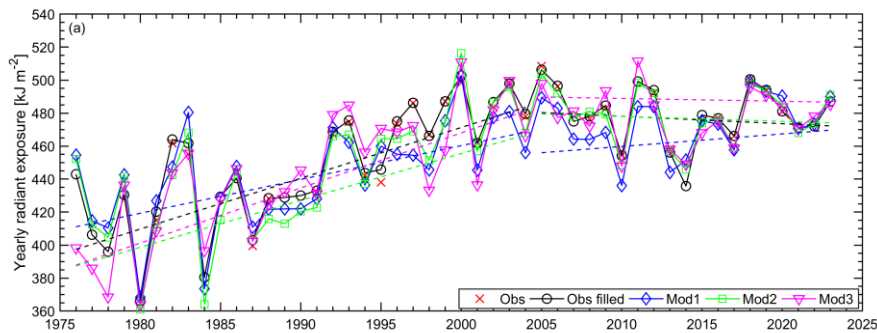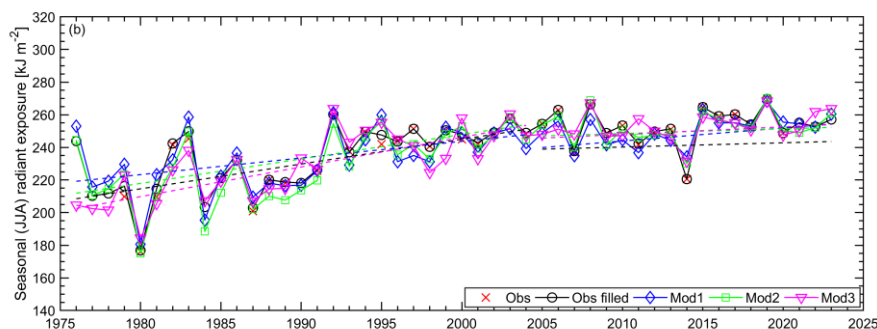
607 **Figure A1. Same as Fig.8, but for the re-evaluated observations with the CC2 correction coefficients.**

608 **Authors contributions**. Conceptualisation, JK and AC; methodology, JK, AC, JJ, PS, and BR; validation, AC
609 and IP; visualisation, AC; writing (original draft preparation), JK and AC; writing (review and editing), JK, AC,
610 PS, and IP; funding acquisition, JK and JJ. All authors have read and agreed to the published version of the paper.

611 **Competing interests**. The contact author has declared that none of the authors has any competing interests.

612 **Acknowledgments**. This work was partially financially by the Chief Inspectorate of Environment Protection,
613 contract number GIOŚ/31/2023/DMŚ/NFOŚ.

614 **References**

615 AERONET: Aerosol Robotic Network: https://aeronet.gsfc.nasa.gov/, last access: 15 April 2025.

616 Berger, D. S.: The sunburning ultraviolet meter: design and performance, Photochem. Photobiol., 24, 587–593,
617 1976.

618 Blumthaler, M., Ambach, W., Morys, M., and Slomka J.: Comparison of Robertson-Berger UV Meters From
619 Innsbruck and Belsk, Publs. Inst. Geophys. Pol. Acad. Sc., D-32 (230), 1989.

620 Borkowski, J. L.: Reevaluation of series of solar UV-B radiation data, Publs. Inst. Geophys. Pol. Acad. Sc., D-48,
621 291, 81–89, 1998.

622 Borkowski, J. L.: Homogenization of the Belsk UV-B series (1976–1997) and trend analysis, J. Geophys. Res.,
623 105(D4), 4873–4878, https://doi.org/10.1029/1999JD900500, 2000.

624 Borkowski, J.L.: Modelling of UV radiation at different time scales, Ann. Geophys., 26, 3, 441–446,
625 https://doi.org/10.5194/angeo-26-441-2008, 2008.

626 Chubachi, S.: Preliminary result of ozone observations at Syowa Station from February, 1982 to January, 1983,
627 Mem. NatI. Inst. Polar Res., Spec. Issue (Jpn), 34, 13–20, 1984.

628 Chubarova, N. Y., and Nezvalʹ, Y. I.: Thirty year variability of UV irradiance in Moscow, J. Geophys. Res., 105,
629 12529–12539, https://doi.org/10.1029/1999JD901192, 2000.

630 Chubarova, N. E., Pastukhova, A. S., Galin, V. Y., and Smyshlyaev, S. P.: Long-Term Variability of UV Irradiance
631 in the Moscow Region according to Measurement and Modeling Data, Izv. Atmos. Ocean. Phys., 54, 139–146,
632 https://doi.org/10.1134/S0001433818020056, 2018.

633 CIE 174:2006: Commission Internationale de l'Eclairage. Action Spectrum for the Production of Previtamin D3
634 in Human Skin. CIE: Vienna, Austria, pp.1–16, 2006.

635 CIE 17166:2019(E): Commission Internationale de l'Eclairage. Erythema Reference Action Spectrum and
636 Standard Erythema Dose. CIE, Vienna, Austria, pp.1-5, 2019.

637 Čížková, K., Láska, K., Metelka, L., and Staněk, M.: Reconstruction and analysis of erythemal UV radiation time
638 series from Hradec Králové (Czech Republic) over the past 50 years, Atmos. Chem. Phys., 18, 1805–1818,
639 https://doi.org/10.5194/acp-18-1805-2018, 2018.

640 Cleveland, W. S.: Robust Locally Weighted Regression and Smoothing Scatterplots, J. Am. Stat. Assoc., 74 (368),
641 829–836, https://doi.org/10.1080/01621459.1979.10481038, 1979.

642 Czerwińska, A., and Krzyścin, J.: Measurements of biologically effective solar radiation using erythemal weighted
643 broadband meters, Photochem. Photobiol. Sci., 23, 479–492, https://doi.org/10.1007/s43630-023-00532-z, 2024a.

644 Czerwińska, A., and Krzyścin, J.: Modeling of Biologically Effective Daily Radiant Exposures over Europe from
645 Space Using SEVIRI Measurements and MERRA-2 Reanalysis, Remote Sens., 16 (20), 3797,
646 https://doi.org/10.3390/rs16203797, 2024b.

647 Dave, J.V. and Halpern, P.; Effect of changes in ozone amount on the ultraviolet radiation received at sea level of
648 a model atmosphere, Atmos. Environ. 10(7), 547-555, https://doi.org/10.1016/0004-6981(76)90181-5, 1976.

649 den Outer, P. N., Slaper, H., Kaurola, J., Lindfors, A., Kazantzidis, A., Bais, A. F., Feister, U., Junk, J., Janouch,
650 M., and Josefsson, W.: Reconstructing of erythemal ultraviolet radiation levels in Europe for the past 4 decades,
651 J. Geophys. Res., 115, D10102, https://doi.org/10.1029/2009JD012827, 2010.

652 Downham, T. F. 2nd: The shadow rule: a simple method for sun protection, South Med J., 91 (7), 619–623, 1998.

653 ERA5:   ERA5   hourly   data   on   single   levels   from   1940   to   present,
654 https://cds.climate.copernicus.eu/datasets/reanalysis-era5-single-levels?tab=overview, last access 15 April 2025.

655 ESRL: The   NOAA   Earth   System   Research   Laboratories,
656 https://www.esrl.noaa.gov/gmd/grad/neubrew/SatO3DataTimeSeries.jsp, last access 6 May 2026.

657 Farman, J., Gardiner, B., and Shanklin, J.: Large losses of total ozone in Antarctica reveal seasonal ClO_x/NO_x
658 interaction, Nature, 315, 207–210, https://doi.org/10.1038/315207a0, 1985.

659 Giovanni: The Bridge Between Data and Science v 4.40: https://giovanni.gsfc.nasa.gov/giovanni/, last access 15
660 April 2025.

661 GMAO: Global Modeling and Assimilation Office, MERRA-2 tavg1_2d_rad_Nx: 2d,1-Hourly, Time-Averaged,
662 Single-Level, Assimilation, Radiation Diagnostics V5.12.4, Greenbelt, MD, USA, Goddard Earth Sciences Data
663 and Information Services Center (GES DISC), https://doi.org/10.5067/Q9QMY5PBNV1T, last access 15 April
664 2025.

665 Gröbner, J., Hülsen, G., Vuilleumier, L., Blumthaler, M., Vilaplana, J. M., Walker, D., and Gill, J. E.: Report of
666 the PMOD/WRC-COST Calibration and Intercomparison of Erythemal Radiometers. Physical Meteorological
667 Observatory Davos World Radiation Center (PMOD-WRC) Pub., 119 pp, Brussels, Belgium, 2009.

Hülsen, G., and Gröbner, J.: Characterization and calibration of ultraviolet broadband radiometers measuring erythemally weighted irradiance, Appl. Opt., 46 (23), 5877–5886, https:/doi.org/10.1364/AO.46.005877, 2007.

Koepke, P., De Backer, H., Bais, A., Curylo, A., Eerme, K., Feister, U., Johnsen, B., Junk, J., Kazantzidis, A., Krzyścin, J., Lindfors, A., Olseth, J. A., den Outer, P., Pribullova, A., Schmalwieser, A. W., Slaper, H., Staiger, H., Verdebout, J., Vuilleumier, L., and Weihs, P.: Modelling solar UV radiation in the past: Comparison of algorithms and input data, Proc. SPIE, 6362, Remote Sensing of Clouds and the Atmosphere XI, 636215, https://doi.org/10.1117/12.687682, 2006.

Koskela T., Taalas, P., and Leszczynski, K.: Correction method for Robertson Berger type ultraviolet radiometer data, Proc. 8th Conference on Atmospheric Radiation, Nashville, Tennessee, USA, 161–163, 1994.

Krzyścin, J. W.: Biologically effective solar radiation (daily radiant exposure and irradiance at noon) at Belsk from 1 January 1976 to 31 December 2023 based on homogenised measurements with broadband radiometers, IG PAS [dataset], https://doi.org/10.25171/InstGeoph_PAS_IGData_Biologically_Effective_Solar_Radiation_Belsk_1976_2023, 2024.

Krzyścin, J. W., and Puchalski, S.: Aerosol impact on the surface UV radiation from the ground-based measurements taken at Belsk, Poland, 1980–1996, J. Geophys. Res., 103 (D13), 16175–16181, 1998.

Krzyścin, J. W., Sobolewski, P. S., Jarosławski, J., Podgórski, J., and Rajewska-Więch, B.: Erythemal UV observations at Belsk, Poland, in the period 1976–2008: Data homogenization, climatology, and trends, Acta Geophys., 59, 155–182, https://doi.org/10.2478/s11600-010-0036-3, 2011.

Krzyścin, J. W., Jarosławski, J., Rajewska-Więch, B., Sobolewski, P. S., Narbutt, J., Lesiak, A., and Pawlaczyk, M.: Effectiveness of heliotherapy for psoriasis clearance in low and mid-latitudinal regions: A theoretical approach, J. Photochem. Photobiol. B Biol., 115, 35–41, https://doi.org/10.1016/j.jphotobiol.2012.06.008, 2012.

Krzyścin, J. W., Sobolewski, P., Czerwińska, A., Rajewska-Więch, B., Jarosławski, J.: Biologically weighted daily radiant exposure for erythema appearance, previtamin D_3 synthesis and clearing of psoriatic lesions from erythema biometers at Belsk, Poland, for the period 1976-2023, PANGAEA [dataset], https://doi.org/10.1594/PANGAEA.972139, 2024.

Leszczynski, K., Jokela, K., Ylianttila, L., Visuri, R., Blumthaler, M.: Erythemally Weighted Radiometers in Solar UV Monitoring: Results from the WMO/STUK Intercomparison, Photochem. Photobiol., 67 (2), 212–221, https://doi.org/10.1111/j.1751-1097.1998.tb05189.x, 1998.

Madronich, S.: UV radiation in the natural and perturbed atmosphere, in: UV-B Radiation and Ozone Depletion. Effects on Humans, Animals, Plants, Microorganisms, and Materials, edited by: Tevini, M., Lewis, Boca Raton, Ann Arbor, London, UK, Tokyo, Japan, 17-69, 1993

Molina, M. J., and Rowland, F. S.: Stratospheric sink for chlorofluoromethanes: chlorine atom-catalyzed destruction of ozone, Nature, 249, 810–812, https://doi.org/10.1038/249810a0, 1974.

NDACC, Network for the Detection of Atmospheric Composition Change, https://www-air.larc.nasa.gov/missions/ndacc/, last access: 15 April 2025.

Neale, R. E., Lucas, R. M., Byrne, S. N., Hollestein, L., Rhodes, L. E., Yazar, S., Young, A. R., Berwick, M., Ireland, R. A., and Olsen, C. M.: The effects of exposure to solar radiation on human health, Photochem. Photobiol. Sci., 22, 1011–1047, https://doi.org/10.1007/s43630-023-00375-8, 2023.

Posyniak, M., Szkop, A., Pietruczuk, A., Podgórski J., and Krzyścin, J.: The long-term (1964-2014) variability of aerosol optical thickness and its impact on solar irradiance based on the data taken at Belsk, Poland, Acta Geophys., 64, 1858–1874, https://doi.org/10.1515/acgeo-2016-0026, 2016.

Puchalski, S.: Preliminary results of the comparison of Robertson-Berger meter with the UV-Biometer MOD 501A, version 3, produced by Solar Light Co., Publs. Inst. Geophys. Pol. Acad. Sc. D-42(269), 113–115, 1995.

Rieder, H. E., Holawe, F., Simic, S., Blumthaler, M., Krzyścin, J. W., Wagner, J. E., Schmalwieser, A. W., and Weihs, P.: Reconstruction of erythemal UV-doses for two stations in Austria: a comparison between alpine and urban regions, Atmos. Chem. Phys., 8, 6309–6323, https://doi.org/10.5194/acp-8-6309-2008, 2008.

Schmalwieser, A. W., Eschenbacher, S., and Schreder, J.: UV-Biometer - The usage of erythemal weighted broadband meters for other biological effects, J. Photochem. Photobiol. B Biol., 230, 112442, https://doi.org/10.1016/j.jphotobiol.2022.112442, 2022.

Scotto, J., Cotton, G., Urbach, F., Berger, D., and Fears, T.: Biologically effective ultraviolet radiation: surface measurements in the United States, 1974 to 1985, Science, 239 (4841), 762–764, https://doi.org/10.1126/SCIENCE.3340857, 1988.

Słomka, J., and Słomka, K.: Comparison of Robertson-Berger ultraviolet meter counts with the UVB and Uver radiation inflow determined from Dave-Halpern's model, Publs. Inst. Geophys. Pol. Acad. Sc., D-22 (189), 133–143, 1985.

Słomka, J., and Słomka, K.: Biologically active solar UV radiation at Belsk in the years 1976-1992, Publs. Inst. Geophys. Pol. Acad. Sc., D-40 (263), 71–81, 1993.

TUV: Tropospheric Ultraviolet and Visible (TUV) Radiation Model: https://www2.acom.ucar.edu/modeling/tropospheric-ultraviolet-and-visible-tuv-radiation-model, last access 15 April 2025.

Volpert, E.V., and Chubarova, N.E.: Long-term changes in solar radiation in Northern Eurasia during the warm season according to measurements and reconstruction model. Russ. Meteorol. Hydro+, 46(8), 507–518, https://doi.org/10.3103/S1068373921080021, 2021.

Weatherhead, E. C., Reinsel, G. C., Tiao, G. C., Meng, X., Choi, D., Cheang, W., Keller, T., DeLuisi, J., Wuebbles, D. J., Kerr, J. B., Miller, A. J., Oltmans, S. J., and Frederick, J. E.: Factors affecting the detection of trends: Statistical considerations and applications to environmental data, J. Geophys. Res., 103 (D14), 17149–17161, https://doi.org/10.1029/98JD00995, 1998.

WMO: World Meteorological Organization, UNEP, Report of the Meeting of Experts on UV-B Monitoring and Research, GORMP-No. 03, WMO, Geneva, Switzerland, 1977.

WOUDC: World Ozone and Ultraviolet Radiation Data Centre, https://woudc.org/data.php, last access 15 April 2025.